Optical trapping of particles at the air/water interface for studies in Langmuir monolayers

A. Gutiérrez-Campos and R. Castillo
Instituto de Física, Universidad Nacional Autónoma de México,
P.O. Box 20-264, Mexico, 01000 D.F.

Recibido el 7 de abril de 2010; aceptado el 8 de junio de 2010

Optical experimental devices allow to observe and manipulate several micron-sized objects, for instance, condensed phase domains formed in Langmuir monolayers at the air/water interface. In this paper, an experimental instrument designed to trap and manipulate those domains is presented. This instrument consists of optical tweezers, colloidal beads as handles and Brewster angle microscopy (BAM) to observe the trapped domains. With this instrument it was possible to trap and observe small domains ($20 - 30$ μm) of nervonic acid monolayers.

Keywords: Optical trapping; optical tweezers; Langmuir monolayers.

Los dispositivos experimentales ópticos permiten observar y manipular diversos objetos de escalas microscópicas como, por ejemplo, dominios de fases condensadas formados en monocapas de Langmuir en la intercara aire/agua. En este artículo se presenta un instrumento experimental diseñado para atrapar y manipular dichos dominios utilizando pinzas ópticas, microesferas coloidales como sujetadores y microscopía de ángulo de Brewster (MAB) para observarlos. Con este instrumento fue posible atrapar y observar dominios pequeños ($20 - 30$ μm) de monocapas de ácido nervónico.

Descriptores: Atrapamiento óptico; pinzas ópticas; monocapas de Langmuir.

PACS: 87.80.Cc; 82.70.Dd

1. Introduction

An optical tweezer is an instrument that uses a tightly focused laser beam to provide an intensity gradient to physically hold and move microscopic dielectric objects. Optical tweezers are invaluable tools to study a wide variety of systems [1]. When a microsphere is attached to a structure of larger size they both can be manipulated by only trapping the microsphere with the tweezers. For instance, domains formed during the growth of condensed phases into liquid phases in Langmuir monolayers, are good examples of structures that can be studied with this technique. Spherical beads have been used by just one group as handles to study Langmuir monolayers domains [2-4].

Amphiphilic molecules that are nearly insoluble in water can form Langmuir monolayers (LMs) at the air/water interface, which are macroscopic systems (formed by $\sim 10^{15}$ molecules) with the only particular property of being one-molecule thick. The most common way to study LMs has been through measurements of the pressure-area isotherms, $\Pi(A,T) = \gamma_0(T) - \gamma(A,T)$, where T is the temperature, A is the area per molecule, and γ and γ_0 are the surface tensions of the monolayer and of pure water, respectively [5]. In the last 20 years, new experimental techniques have revealed that many of the singularities observed in surface pressure-area isotherms, since the works of Stenhagen [6] and Ludquist [7,8], are due to phase changes, where each phase can be described in terms of four order parameters [9]. In particular, one of the techniques that has been developed to study monolayer organization is the Brewster angle microscopy (BAM) [10, 11]. It provides information about homogeneity, texture, structure, and dynamics at large scales ($2-500$ μm). BAM is a noninvasive optical technique that is quite sensible for observing very fine details during phase transformations, and it is probably the best suited to be used in direct observations during monolayer compression or expansion. BAM is based on the study of the reflected light coming from an interface illuminated at the Brewster angle, by a p-polarized laser beam. When the angle of incidence of this beam is at the Brewster angle, the reflected intensity is a minimum for a real interface, which has a transition region where the refractive index changes smoothly from one value to another. The reflected intensity at this angle is strongly dependent on the interfacial properties, mostly when a monolayer is involved in the interface. The reflectivity has three origins:

(a) the thickness of the interface;
(b) the roughness of the real interface due to thermal fluctuations;
(c) the anisotropy of the monolayer.

Reflected light is a function of the orientation of the molecules in monolayer domains. In tilted phases, the anisotropy is relatively strong producing enough light reflection to make quite visible the mosaic of textures due to tilted domains in different directions. In untilted phases with rectangular lattice symmetry, textures are also visible, but with much less contrast. On the other hand, multilayer structures reflect very large quantities of light as compared with monolayers.

Recently, a study of how patterns formed by monolayer domains of a stable phase, usually solid or liquid condensed (LC); propagate into a metastable one, usually liquid expanded (LE), has been presented [5,12,13]. During this prop-

agation, the line interface between the two phases moves as the metastable phase is transformed into the more stable one. The line interface becomes unstable and forms patterns because of the competition between a chemical potential gradient that destabilizes the interface, on the one hand and line tension that stabilizes the interface, on the other hand. The further the system is out of equilibrium, the faster the metastable phase will turn into the stabler phase and, consequently, the faster the interface will propagate. The competition between effects that stabilize and destabilize the line interface gives rise to characteristic length scales of growing domains which determine, together with the anisotropy, the overall shape and symmetry of the domains. This kind of studies have motivated our group to design and assemble an optical tweezer to help in the manipulation of domains during their growth which, in turn, can be controlled experimentally.

It is possible to deposit, together with the monolayer, microspheres with an index of refraction higher than that of the surrounding medium. During monolayer compression, these microspheres become nucleation centers, staying attached to the domains. On this way, it is possible to manipulate both: the microsphere and the domain, using optical tweezers. Recently, Th. M. Fischer *et al*. [2] have developed a novel technique to manipulate Langmuir monolayer domains with optical tweezers in combination with BAM and fluorescence microscopy. With this technique they achieved thermal and mechanical micromanipulation of monolayers using silica and polyethylene (PE) microspheres. They also measured the line tension of liquid expanded/gas-phase boundary of methyl octadecanoate Langmuir monolayers by deforming the boundary with the tweezers [3], or, by observing a fixed domain deformed by the hydrodynamic flow of the surroundings [4].

In this paper, an instrument to study Langmuir monolayers based on optical tweezers combined with BAM is reported. The lens objective to form the tweezers is not immersed in the subphase as in previous designs [2-4]. This instrument allows to trap microspheres deposited at the air/water interface and, at the same time, monolayers deposited together with the microspheres can be observed. The principles of optical trapping are briefly reviewed in Sec. 2. In the subsequent Sections, a detailed description of the experimental setup, with examples showing trapped nervonic acid domains, are presented.

2. Principles of optical trapping

An optical tweezer is an optical trap that uses the forces produced by a sharply focused beam to manipulate objects, with size ranging from $\sim$ 10 nm to $\sim$ 10 μm, and with index of refraction higher than that of the surrounding medium. Usually, a microscope objective of high numerical aperture (NA) is used to concentrate the incident light in a small diffraction-limited spot. If the incident beam overfills the objective entrance pupil by using, for instance, a beam expander, the spot will be smaller.

Although theories behind optical tweezers are still in progress, the basic principles are straightforward for objects either much smaller, or much larger, than the wavelength of the incident beam. Small objects develop an electric dipole moment as a response to the light's electric field, which, usually has intensity gradients in the electric field toward the focus. Larger objects behave as lenses, refracting the optical rays and redirecting the momentum of their photons [1, 14]. Therefore, two regimes can be distinguished. In both cases, the optical forces involved can be divided into two groups:

(i) the forces arising from scattering of the incident beam, and
(ii) the forces arising from an intensity gradient [15].

2.1. Small objects regime: electromagnetic field approximation

In cases where the diameter of the trapped particle is much smaller than the wavelength of the beam λ, the conditions for Rayleigh scattering are satisfied and the particle can be treated as a point dipole in an inhomogenous electromagnetic field [16]. In this case, the scattering force is due to absorption and reradiation of light by a dipole. For a spherical particle, this force is in the same direction of propagation of the incident light, and proportional to its intensity. This means that the incident light pushes the particle in the direction of propagation of the beam [17, 18].

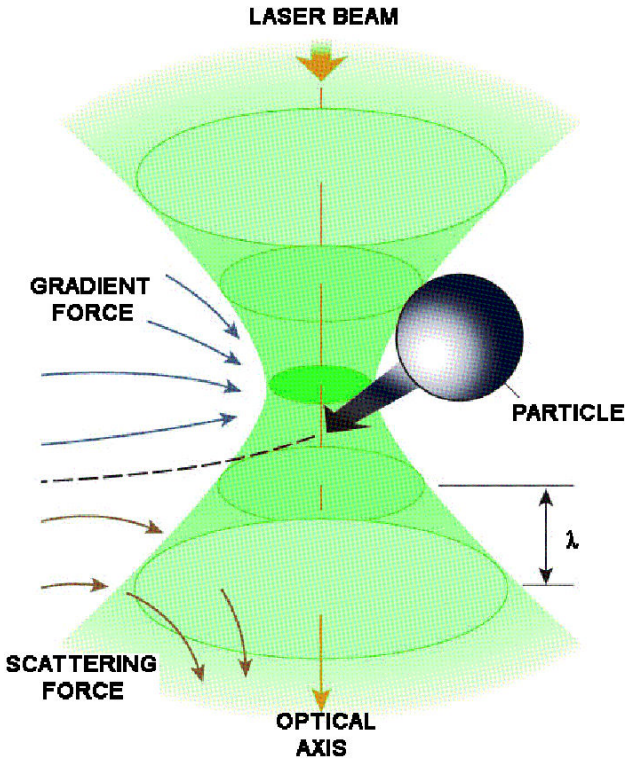

FIGURE 1. In the electromagnetic approximation the particles are drawn toward the beam focus by virtue of the gradient force, whereas the scattering force tends to move the particles along the optical axis. Adapted image from Ref. 14.

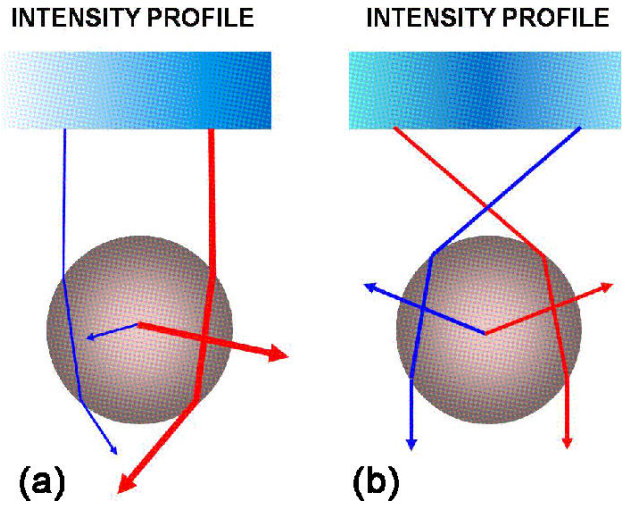

FIGURE 2. Ray optics to represent the gradient force: (a) gradient intensity increasing from left to right, and (b) radial intensity gradient. In the latter case the optical trap is stable. Adapted image from Ref. 17.

On the other hand, the gradient force is a consequence of the fact that a dipole in an inhomogeneous electromagnetic field experiences a force in the direction of the field gradient [16]. In optical tweezers, the incident beam induces fluctuating dipoles in dielectric particles, and the gradient trapping force arises when these dipoles interact with the inhomogeneous electromagnetic field [17]. In this case, the gradient force is proportional to the intensity gradient and points in the same direction as the gradient when the index of refraction of the particle is higher than that of the surrounding medium [17, 18].

The scattering force acts in the same direction as the beam, whereas the gradient force acts toward the beam focus. It is straightforward to note that for a beam directed downwards the stable trapping point is located below the focus. Therefore, for a stable three-dimensional trap, it is necessary that the gradient force exceeds the magnitude of the scattering force [18]. In Fig. 1, scattering and gradient forces are shown.

2.2. Large objects regime: ray optics approximation

When the trapped particles are much larger than the wavelength of the incident beam, the forces can be calculated from ray optics. The incident light is refracted by the particle, and the momentum carried by the light changes. By Newton's third law, an equal and opposite momentum change on the sphere ensues. Thus, the force acting on the sphere is proportional to the intensity of the light. If the index of refraction of the particle is higher than that of the surrounding medium, the optical force coming from refraction is in the intensity gradient direction. On the contrary, if the index is smaller than that of the medium, the force is in the opposite direction of the intensity gradient [17, 18]. From ray optics, and for a spherical particle, it can be shown that the extreme rays contribute the most to the axial gradient force, and the central rays are mainly responsible for the scattering force. It can also be shown that the stable trapping point is located just below the focus for a beam directed downwards. In Fig. 2 two light intensity profiles are shown. In (a), a sphere is illuminated by a beam with an intensity gradient increasing from left to right. The two refracted rays shown in the image have different intensities. The sphere experiences a momentum change represented by the two vectors pointing outwards from its center. The effect of this intensity gradient on the particle is a net displacement toward the right and slightly down. The particle is not trapped. In (b) a radial intensity gradient is represented. In this case, the sphere is trapped in three dimensions by virtue of the configuration of the incident beam.

3. Experimental techniques

In this section, the techniques and instruments used to assembly the complete experimental setup to trap monolayer domains with the optical tweezers are described.

Optical system. To form the optical tweezers, a microscope objective $100\times$ (Mitutoyo M plan APO, NA 0.7, working distance of 6 mm) was used. The optical trap was created from a single beam of laser light at wavelength $\lambda = 514.5$ nm provided by an Ar laser (Stabilite 2017, Spectra Physics, U.S.A.). A beam expander (model 09 LBZ 001 Melles Griot, U.S.A.) was used to fill the back aperture of the microscope objective. To illuminate the beads to be trapped, a fiber optic illuminator (Cole-Parmer model EW-09790-00, U.S.A.) of cold white light was used. Additionally, a special set of lenses and mirrors used to manipulate the tweezers was mounted. To observe the trapped particles at the air/water interface a Modular Magnification System (Edmund models 55-908 MMS R4, and MMS OBJ-7 55-901, U.S.A.) was connected to a video camera (High Performance Vidicon Camera, modelo C2400-01, Hamamatsu, Japan). The camera was connected to a monitor (Sony Trinitron model SSM-14N5U, Japan), and to a video recorder (Mitsubishi VHS Hi-Fi model HS-U48, Japan).

Beam waist measurements. To measure the laser beam waist a photosensor (model H5784-04, Hamamatsu, Japan) was used. Perpendicular to the laser beam, a knife-edge was placed on a XY micropositioner.

Isolation system. The experiment was placed on an optical table (model 13811, Oriel Corporation, U.S.A.), to avoid external vibrations, and to keep the optical system aligned. Additionally, the experiment was put inside of a 1 m^3 plastic box to avoid undesired air convection.

Langmuir trough. A rectangular NIMA trough (601 M, Nima Technology Ltd., England) made of PTFE, with a working area starting at 84 cm^2, was used. The trough is supplied with a sapphire UV-Visible transmission window for inverted microscopy where the laser beam that forms the tweezers enters with the aid of the high numerical aperture microscope objective. The temperature difference between the surroundings defined by the air inside the box and the trough was at most $1°C$. A Wilhelmy plate was used to measure the lateral pressure, Π, and temperature was kept constant with the aid of a water circulator bath (Cole-Parmer 1268-14 U.S.A.). All experiments were carried out in a clean-room lab.

Amphiphiles. Nervonic acid (NA) ($\geq$ 99%) was obtained from Sigma Aldrich Inc. (MO, U.S.A.). It was used without further purification.

Monolayer. Measurements of the pressure-area isotherms were performed spreading the amphiphiles in solution onto a subphase made of ultrapure water (Nanopure-UV, 18.3 MΩ, U.S.A.) in a Langmuir trough. T is the temperature, A is the area/molecule, γ and γ_0 are the surface tensions of the monolayer and of the uncovered subphase, respectively. The spreading solution was made with chloroform (HPLC, Aldrich, U.S.A.) at a concentration of 1 mg/mL. The NA monolayers were worked at pH $5.7 - 5.8$. After a waiting time ($15 - 20$ minutes) for allowing evaporation of the solvent coming from the spreading solution, the monolayer was slowly compressed.

BAM. The growth of domains was observed with an Elli2000 imaging ellipsometer (Nanofilm Technologie GmbH, Germany) in the BAM mode (spatial resolution of $\sim$ 2 μm). When the monolayer moved slowly, this instrument allowed us to get observations with the whole field of view in focus, due to its movable objective lens.

Microspheres. Silica beads (with silanol (SiOH) surface groups) were purchased from Bangs Laboratories, Inc. (U.S.A.) with a mean diameter of 2.47 μm (10 wt%, solids). The density of the microspheres is 2.0 g/cm^3, avoiding flotation on the subphase. However, if beads are treated with $8 - 10$ times centrifugation-sonication cycles in a chloroform-ethanol mixture, they end up hydrophobized, allowing them to float on the air/water interface. A 1 wt% bead suspension in a 1:1 chloroform-ethanol mixture was prepared. 80 μL of this suspension were mixed with 5 mL of the monolayer spreading solution. This new suspension is the actual spreading solution to deposit amphiphiles and microspheres at the same time on the air/water interface. To test the optical tweezers, polystyrene microspheres, with mean diameters of 9.00 and 2.00 μm (Bangs Laboratories, Inc., U.S.A.), were used (9.9 and 10 wt% solids, respectively). These beads were cleaned with $8 - 10$ times centrifugation-sonication cycles in ethanol. The size of the beads ranges between 2.00 and 9.00 μm in diameter. Therefore, the ray optics approximation explained above may be used to describe the forces exerted by the tweezers.

4. Beam waist measurement

Before setting up the tweezers, measurements of the beam waist, after the light has passed through the microscope objective, were performed. The original laser beam is Gaussian, and it preserves its shape after passing through the objective (see, for instance, Ref. 19). A beam with such a characteristic has an intensity distribution described by a Gaussian function depending on the beam propagation direction z, and on the radial distance ρ,

$$I(\rho, z) = I_0 \left[\frac{W_0}{W(z)}\right] \exp\left(-\frac{2\rho^2}{W^2(z)}\right), \qquad (1)$$

where $W(z)$ is the beam radius (or the beam width). It assumes its minimum value W_0 in the plane $z = 0$, called the beam waist. Thus W_0 is the waist radius. In that region the wavefronts are nearly flat and they become spherical away from the waist. W_0 is a function of the laser wavelength. If the beam waist, $W(z) = W_0$, is located at $z = 0$ the intensity is given by [20, 21]

$$I(x, y) = \frac{2P_0}{\pi W_0^2} \exp\left(-\frac{2(x^2 + y^2)}{W_0^2}\right), \qquad (2)$$

where $\rho = \sqrt{x^2 + y^2}$. The method to determine the beam waist consists of the measurement of the power past a knife-edge which is slowly inserted in the beam, as shown in Fig. 3. This is perpendicular to the direction of propagation of the beam. The power P transmitted past the knife-edge blocking off all points for which $x \leq a$ (see inset in Fig. 3) is given by [21]

$$P = \int_{-\infty}^{\infty} \int_{a}^{\infty} I(x, y)\, \mathrm{d}x\, \mathrm{d}y = \frac{P_0}{2} \mathrm{erfc}\left(\frac{a\sqrt{2}}{W_0}\right), \qquad (3)$$

where P_0 is a constant, and erfc() is the complementary error function [20]. If power is measured for different positions of the knife-edge, it is possible to plot P as a function of a, and therefore, one can obtain W_0 through Eq. (3).

With the experimental set up shown in Fig. 3, the voltage (which is proportional to the power) of the beam past the microscope objective was measured. The knife-edge was placed on a XY micropositioner. The voltage was measured with a photosensor. In Fig. 4, plots of voltage as a function of the knife-edge position are shown. The experimental data (squares) were obtained by inserting the knife-edge in the beam past the objective. The solid line is the fitted curve

using Eq. (3). The inset shows a similar plot for the beam before the microscope objective. On average, the beam waist past the objective is 56 ± 7 μm, whereas the beam waist before the objective is 3.6 ± 0.086 mm.

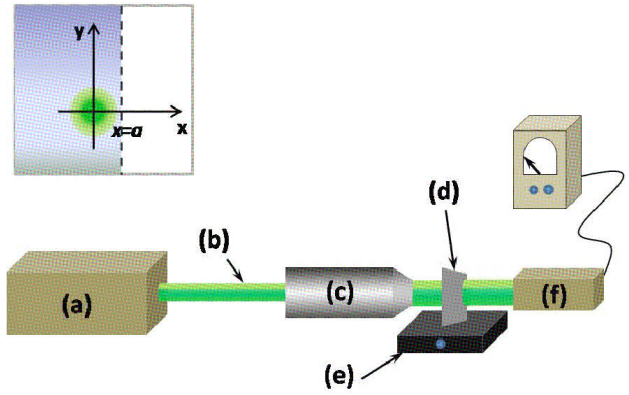

FIGURE 3. Experimental setup to measure the beam waist: (a) laser, (b) beam, (c) microscope objective, (d) knife-edge, (e) XY micropositioner, (f) photosensor. Inset: semi-infinite plane, placed at $x = a$, representing the knife-edge. The laser beam is along the z axis.

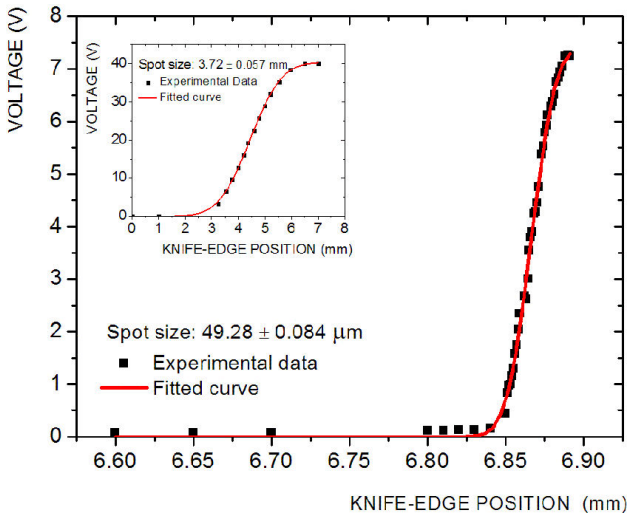

FIGURE 4. Voltage vs knife-edge position. The knife was placed at the objective working distance, *i.e.* the focal plane. The squares correspond to the experimental points, whereas the solid line is the fitted curve using Eq. (3). The inset shows the same kind of plot for the beam before the objective.

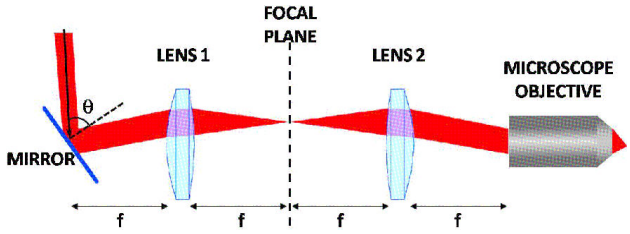

FIGURE 5. Afocal telescope formed with two converging lenses of focal distance f and a beam steering mirror. This system is used to manipulate the trapped objects. Adapted image from Ref. 18.

5. Experimental setup

In this section, the experimental details of the instrument (tweezers, trough and BAM) assembly will be described.

5.1. Optical tweezers

The basic optical components to assembly the tweezers are: a trapping laser and a microscope objective as described en Sec. 3. It is also convenient to use an afocal telescope to manipulate the beam. The microscope objective has two functions:

(i) it is the most important element of the tweezers, since it determines the overall efficiency of the optical trapping system. Due to its high magnification and numerical aperture, one can obtain a small diffraction-limited spot.

(ii) It forms a real, inverted image 100 times magnified in the focal plane.

Since the objective is apochromatic, the tweezers are more efficient. The incident laser beam has to overfill the back aperture of the objective lens as a requirement to obtain the smallest possible focused spot, and therefore, steeper intensity gradient; a beam expander was used.

The afocal telescope [22] is an optical array consisting of two converging lenses and a beam steering mirror to manipulate the trapped object. This system has to produce a collimated laser beam which is always centred on the back aperture of the objective lens. An angular displacement about the beam center will produce a lateral displacement of the focused spot in the sample plane [18]. In Fig. 5 an afocal telescope diagram is shown. It is formed with two converging lenses with focal distance f and a beam steering mirror: the collimated laser beam incides at some angle θ upon the mirror located at a distance f from the first lens. Past the first lens, the reflected beam focuses in the focal plane located halfway between the two lenses. The two lenses are $2f$ apart. From this plane, the beam diverges toward the second lens, where the beam emerges parallel. At a distance f from this lens, the beam center hits the optical axis, where the back pupil of the objective is found. So, if the beam is moved through the mirror, the back pupil will be still overfilled. In front of the objective, the beam will emerge slightly deviated from the optical axis. This deviation can be controlled on a micrometer scale with a kinematic optic mount. Two plano-convex lenses with $f = 150$ mm were used.

The laser beam trajectory can be modified if different optical components are inserted, for instance, between the second lens and the objective, as shown in Fig. 6. A dichroic mirror, reflecting the laser wavelength at $45°$, and transmitting the rest, was used. Thus, the laser beam is reflected in the dichroic mirror (DM1), then it enters the microscope objective and forms the tweezers 6 mm above the objective, where the sample plane is located. In that plane, part of the light is

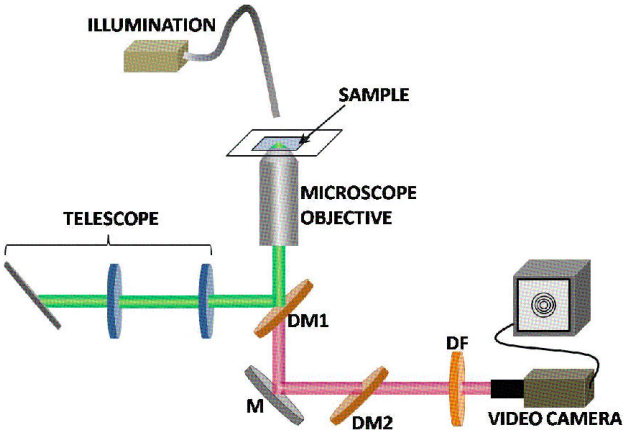

FIGURE 6. Optical tweezers diagram. An infinity corrected microscope objective was used.

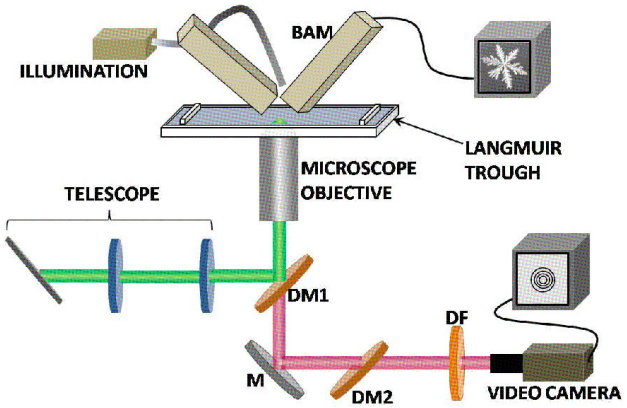

FIGURE 7. Experimental setup diagram. The Langmuir trough was resting on an aluminum table (not shown) to place it just above the microscope objective. In front of the BAM objective the narrow bandpass interference filter was placed.

transmitted and part reflected. The latter is reflected once again by mirror DM1, where 90% of this light returns in direction of the telescope. The remaining 10% is transmitted through DM1 and is blocked with another dichroic mirror (DM2) and with a dichroic filter (DF). Thus, the light coming from the tweezers is almost totally blocked before arriving to the video camera used to observe the trapped particles.

On the other hand, it is necessary to use an additional illumination source to observe the trapped particles. This has to be placed above the sample, as shown in Fig. 6. In this case, a cold white light was used. This lamp does not cause an important warming of the sample. The light coming from the illumination system travels to the video camera after being filtered by two dichroic mirrors (DM1 and DM2) and a filter (DF). The video camera was coupled to a modular magnification system, as described in Sec. 3, to obtain an additional magnification and an infinity-corrected system. To determine the magnification of the complete system, a calibration grid located on the sample plane was used. The measured magnification was found to be $\sim 4000\times$.

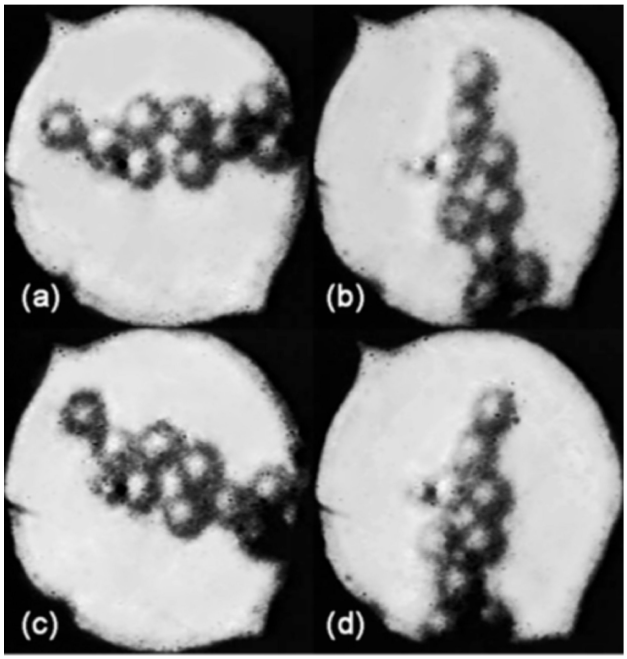

FIGURE 8. Images of a cluster of 9.00 μm polystyrene beads trapped with the tweezers, in an air/water interface in a Langmuir trough, observed with the tweezers video camera at (a) $t = 0$ s, (b) $t = 32$ s, (c) $t = 96$ s, and (d) $t = 140$ s.

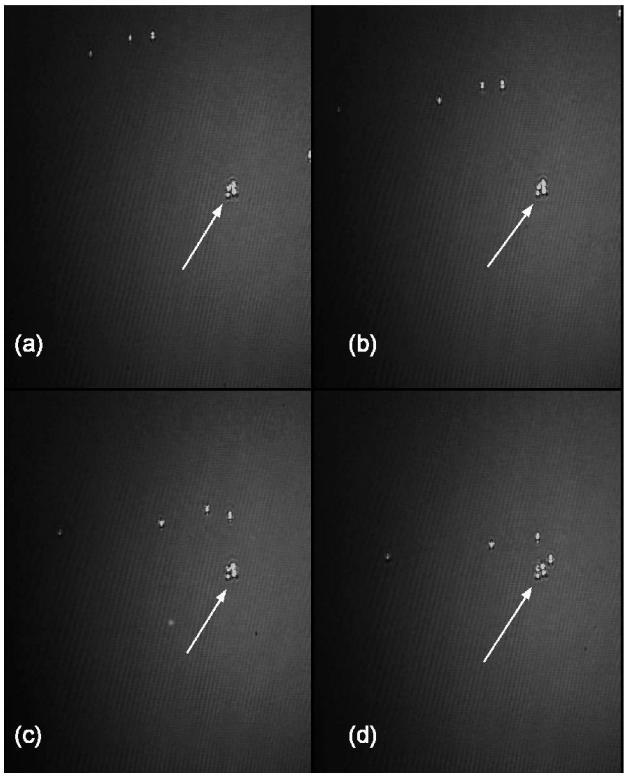

FIGURE 9. BAM images of a cluster of polystyrene beads (9.00 μm) trapped with the tweezers in an air/water interface on a Langmuir trough at: (a) $t = 0$ s, (b) $t = 10$ s, (c) $t = 20$ s, y (d) $t = 30$ s. The horizontal full width is 460 μm, for each image.

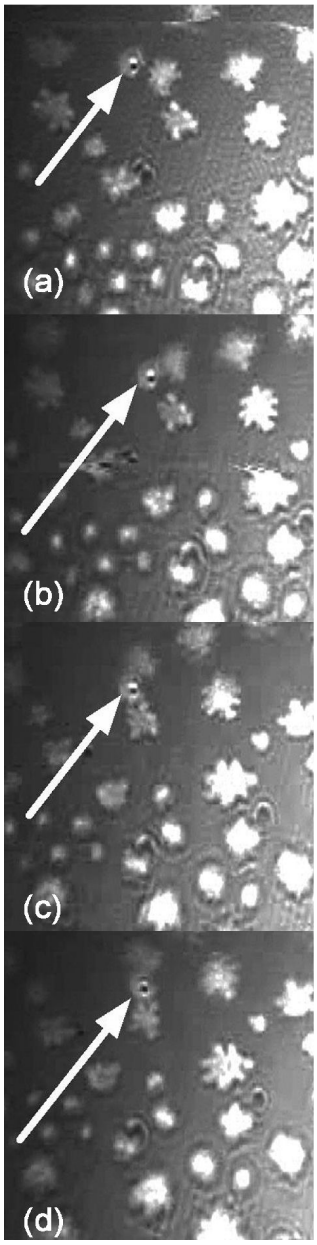

FIGURE 10. BAM images of a silica bead, attached to a nervonic acid domain, captured by the optical twezers in the place pointed by the arrow. Images were taken each 0.48 s. Horizontal full width 245 μm, for each image.

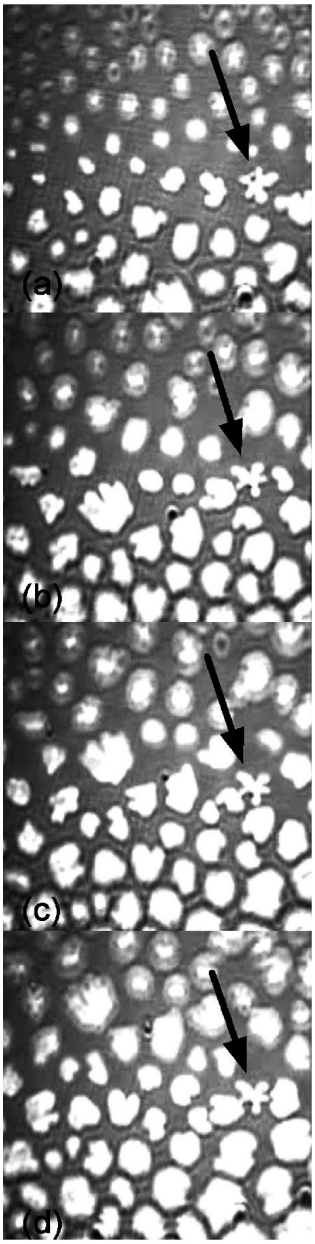

FIGURE 11. BAM images of a silica microsphere trapped. When a domain is near the microsphere, they interact. The domain rotates about the trapping point due to the monolayer flow. The images were taken each 6 s. Horizontal full width 245μm, for each image.

To test the optical tweezers, a cell consisting of two glass cover slips, glued to each side with Mylar® (polyethylene tereftalate) spacers, was used. The cell was filled with polystyrene beads (2.00μm diameter) in suspension (0.1 wt%) of ultrapure water. A Z micropositioner was used to move vertically the cell to determine that the trapping point is located 80μm above the focus. The laser power required to trap these microspheres is $\geq$ 40 mW. The maximum lateral displacement of the tweezers, that can be obtained with the beam steering mirror, was found to be $\sim 50\mu$m.

5.2. Langmuir trough and BAM mounting

To couple the Langmuir trough with the optical system described above, a height adjustable aluminum table, with a hole in the center, was used. With this table it was possible to place the trough's transmission window just above the microscope objective. Then, the BAM was placed above the trough to observe the air/water interface. The complete experimental setup is shown in Fig. 7.

The light coming form the laser beam is partially trans-

mitted at the air/water interface, and it is detected by the BAM objective. This light excess coming from the tweezers avoids the interface observation, and therefore, a narrow bandpass interference filter (FWHM 3 nm) centered on the BAM laser wavelength (532 nm) was required, so the light detected by the BAM objective comes from the BAM itself and not from the optical tweezers.

6. Results and discussion

Once the experimental setup was mounted, the optical tweezers were tested with polystyrene beads (9.00 μm diameter). The beads were deposited on an air/water surface of ultrapure water, at pH 5.7 and at room temperature (22°C). In these conditions, a cluster of beads was trapped with the tweezers, with a laser power of 500 mW. In Fig. 8 four successive images acquired with the tweezers video camera are shown. As time elapses from $t = 0$ s to $t = 140$ s, the cluster rotates about the trapping point.

The trapped particles can be observed with the BAM at the air/water interface. In this case, the tweezers and the BAM field of view alignment is critical. In Fig. 9, four successive BAM images of a cluster of polystyrene beads (9.00 μm) trapped with the tweezers are shown. The arrows indicate the tweezers position. Here, it is easy to see how particles not trapped are moving with respect to the trapped cluster. In this case, the subphase pH is 5.7, at room temperature $T = 22^{\circ}$C, and a laser power 400 mW.

With the experimental setup described, a nervonic acid monolayer mixed with silica beads (2.47 μm) was deposited onto an air/water interface. The subphase pH was 5.7 and at room temperature $T = 22^{\circ}$C. The monolayer was compressed at relatively low speed ($6\,\mathrm{cm}^2/\mathrm{min}$). At this temperature, the nervonic acid monolayer shows a coexistence region of liquid expanded (LE) and liquid condensed (LC) phases, at lateral pressures of ~ 3 mN/m [12]. Above this pressure, LC domains, with sizes ranging between $20 - 500\mu$m, start to grow. The silica microspheres are initially dispersed in the LE phase. As monolayer compression takes place, some of these microspheres become nucleation centers for LC domains, whereas the rest remains dispersed in the LE phase. To trap a single domain with the tweezers it is required to trap one of the microspheres that have become a nucleation center. An example is shown in Fig. 10, where a small domain (~ 20 μm) is trapped with the tweezers (see arrow). Four successive images were taken each 0.48 s. The surrounding domains interact with the trapped domain up to the point of detaching it from the optical tweezers (not shown).

Another possibility, is to trap one of the microspheres dispersed in the LE phase, and to wait for the moment when an interaction of a domain with the microsphere takes place, as shown in Fig. 11. In this case, four successive images were taken each 6 s. Notice that the microsphere is located in the space between two arms of the domain. It rotates by virtue of the monolayer flow and the interaction between domains. Finally, the domain is dragged away from the optical tweezers (not shown).

7. Concluding remarks

A technique, based on optical tweezers, to trap colloidal particles at the air/water interface which interact with phase condensed domains of Langmuir monolayers was developed. Direct observation of the monolayers was made with a BAM. To trap the domains, their size has to range between $20-30$ μm, otherwise the tweezers are not strong enough to trap them. It was also noticed that interaction between other not trapped domains, may cause the trapped domain to be detached from the tweezers, so it would be convenient to trap isolated domains. The laser power should be as low as possible, since it was observed that for powers > 800 mW, the microspheres are warmed up to the point to melt the LC domains, and it seems as they are "erased" with the microsphere. The laser power should range between $400 - 600$ mW for a good trap.

Finally, it should be mentioned that this technique, apparently, may have further applications to studies in monolayers, such as to perform viscosity measurements, or studies in dipolar interactions. On the other hand, it can be used to study the dynamics of Janus particles at the air/water interface [23]. However, it should be pointed that it would be convenient to improve the tweezers, for instance, with a microscope objective with a higher numerical aperture. This may generate a stronger optical trap. The experimental setup described in this paper may be appropriate to study pattern formation in monolayers forming small domains, such as dioctadecylamine, DMPE, or DPPC.

Acknowledgment

The support from SEP-CONACYT (81081) and DGAPA-UNAM (112508) is gratefully acknowledged. We also thank to C. Garza and S. Ramos for their technical support in optical alignment and monolayer development.

1. A. Ashkin, *Optical trapping and manipulation of neutral particles using lasers* (Word Scientific, E.U.A., 2006).

2. S. Wurlitzer, C. Lautz, M. Liley, C. Duschl, and Th. M. Fischer, *J. Phys. Chem. B* **105** (2001) 182.

3. S. Wurlitzer, P. Steffen, and Th. M. Fischer, *J. Chem. Phys.* **112** (2000) 5915.

4. S. Wurlitzer, P. Steffen, M. Wurlitzer, Z. Khattari, and Th. M. Fischer,*J. Chem. Phys.* **113** (2000) 3822.

5. A. Flores, E. Corvera-Poiré, C. Garza, and R. Castillo, *J. Phys. Chem. B* **110** (2006) 4824.
6. E. Stenhagen, *Determination of organic structures by physical methods* (Academic Press, Nueva York, E.U.A., 1955).
7. M. Lundquist, *Chemica Scripta* **1** (1971) 197.
8. M. Lundquist, *Prog. Chem. Fats other Lipids* **16** (1978) 101.
9. V.M. Kaganer, H.Möhwald, and P. Dutta, *Rev. Mod. Phys.* **71** (1999) 779.
10. S. Hénon and J. Meunier, *Rev. Sci. Instrum.* **62** (1991) 936.
11. D. Hönig and D. Möbius, *J. Phys. Chem.* **95** (1991) 4590.
12. A. Gutiérrez-Campos, G. Díaz-Leines, and R. Castillo, *J. Phys. Chem. B* **114** (2010) 5034.
13. A. Flores, E. Corvera-Poiré, C. Garza, and R. Castillo, *Europhys. Lett.* **74** (2006) 799.
14. D.G. Grier, *Nature* **424** (2003) 21.
15. A. Ashkin, J.M. Dziedzic, J.E. Bjorkholm, and S. Chu, *Optics Lett.* **11** (1986) 288.
16. J.D. Jackson, *Classical Electrodynamics* (John Wiley, Nueva York, E.U.A., 1999).
17. K.C. Neuman and S.M. Block, *Rev. Sci. Instrum.* **75** (2004) 2787.
18. J.E. Molloy and M.J. Padgett, *Contemp. Phys.* **43** (2002) 241.
19. J.W. Goodman, *Introduction to Fourier Optics* (McGraw Hill, E.U.A., 1996).
20. B.E.A. Saleh and M.C. Teich, *Fundamentals of photonics* (J. Wiley, E.U.A., 2001).
21. R.S. Sirohi, *A course of experiments with He-Ne laser* (J. Wiley, E.U.A., 1985).
22. E. Hecht, *Optics* (Addison-Wesley, E.U.A., 1987).
23. S. Jiang *et al.*, *Adv. Mater.* **22** (2010) 1060.